Electronic Supplementary Information

High efficiency Bi_2Te_3-based materials and devices for thermoelectric power generation between 100 and 300 ˚C

Feng Hao[ab], Pengfei Qiu[a], Yunshan Tang[a], Shengqiang Bai*[a], Tong Xing[ab], Hsu-Shen Chu[c], Qihao Zhang[ab], Ping Lu[a], Tiansong Zhang[a], Dudi Ren[a], Jikun Chen[d], Xun Shi*[ae], Lidong Chen*[ae]

[a] State Key Laboratory of High Performance Ceramics and Superfine Microstructure, Shanghai Institute of Ceramics, Chinese Academy of Sciences, Shanghai 200050, China.

[b] University of Chinese Academy of Sciences, 19 Yuquan Road, Beijing 100049, China.

[c] Material and Chemical Research Laboratories, Industrial Technology Research Institute, Hsinchu 31040 Taiwan.

[d] School of Material Science and Engineering, University of Science and Technology Beijing, Beijing 100083, China.

[e] Shanghai Institute of Materials Genome, Shanghai 200444, China.

Lattice thermal conductivity (κ_L) and bipolar thermal conductivity (κ_b)

The κ_L data at 200-250 K was fitted by the expression of $\kappa_L = aT^{-1} + b$, where a and b are fitting parameters. As a typical example, Fig. S4c shows the fitting results for $Bi_{0.5}Sb_{1.5}Te_3$. Very good agreement between the experiment data and the fitting curve (red solid line) is observed. Similar agreements are also observed in all other samples. The fitted a and b values for the samples are listed in Table S1. The κ_L was then extrapolated to 600 K according to the expression $\kappa_L = aT^{-1} + b$, which is shown in Fig. S4d. For sample $Bi_{0.5}Sb_{1.485}Cd_{0.015}Te_3$, $Bi_{0.5}Sb_{1.495}Cu_{0.005}Te_3$, and $Bi_{0.5}Sb_{1.494}Ag_{0.006}Te_3$, the κ_L at elevated temperatures are lower than the theoretical minimum lattice thermal conductivity (κ_{min} = 0.31 $Wm^{-1}K^{-1}$) in $Bi_{0.5}Sb_{1.5}Te_3$ calculated by the Cahill model.[1] In this case, κ_{min} is used as the real κ_L value instead of the extrapolated value. Finally, the κ_b for all the samples at 300-600 K was calculated by subtracting the estimated κ_L from experimental (κ - $L\sigma T$).

In n-type Bi_2Te_3–based materials, acoustic phonon scattering is also the dominant carrier scattering mechanism around 300 K. Thus, the electron mobilities (μ_e) also obey the relationship of $\mu_e \sim T^{-3/2}$.[2] Based on Fig. 4a, we found that the calculated electron concentrations (n) for all samples varies as with the empirical relationship of $n \sim T^7$. Thus, a qualitative expression between μ_e and n is derived as $\mu_e \approx Bn^{-1/5}$, where B is a temperature independent constant for a fixed composition. Then the electron

partial electrical conductivity σ_e is calculated based on parameter B and electron concentrations.

In the following numerical modeling process, B is set as an adjustable parameter and listed in Table S3. Then, Equation 7 is approximately changed to

$$\kappa_b = \left(\frac{k_B}{e}\right)^2 T\left(4 + \frac{E_g}{k_B T}\right)^2 \cdot \frac{Bn^{\frac{4}{5}} \cdot p\mu_h}{Bn^{\frac{4}{5}} + p\mu_h}, \quad \text{(S1)}$$

where e is the free electron charge, μ_h (= μ_H) is the hole mobility, and p (= p_H) is the hole concentration. The μ_h above 300 K can be extrapolated by using the measured low temperature Hall data according to the relationship of $\mu_h(T) \sim T^{-3/2}$. The p values above 300 K were calculated using Equation 6. Then, the temperature dependence of κ_b was modeled by Equation S1, which is shown in Fig. S8a. Excellent agreements between the calculations using the experimental data ($\kappa_b = \kappa - \kappa_e - \kappa_L$, symbols) and the fitted curves using Equation S1 (solid lines) are observed in a wide temperature range for all samples, suggesting the assumption and augment mentioned above is reasonable.

Lorenz number (L)

Lorenz number is calculated by using the single parabolic band model according to the following expression[3]

$$L = \left(\frac{k_B}{e}\right)^2 \left\{ \frac{(\lambda + 7/2)F_{\lambda+5/2}(\eta_h)}{(\lambda + 3/2)F_{\lambda+1/2}(\eta_h)} - \left[\frac{(\lambda + 5/2)F_{\lambda+3/2}(\eta_h)}{(\lambda + 3/2)F_{\lambda+1/2}(\eta_h)}\right]^2 \right\} \quad \text{(S2)}$$

where λ is the carrier scattering parameter which is taken as -1/2, η_h is the reduced Fermi energy, F_x is the Fermi integral of the order of x. The calculated values for our materials are listed in Table S1.

Electronic Supplementary Information

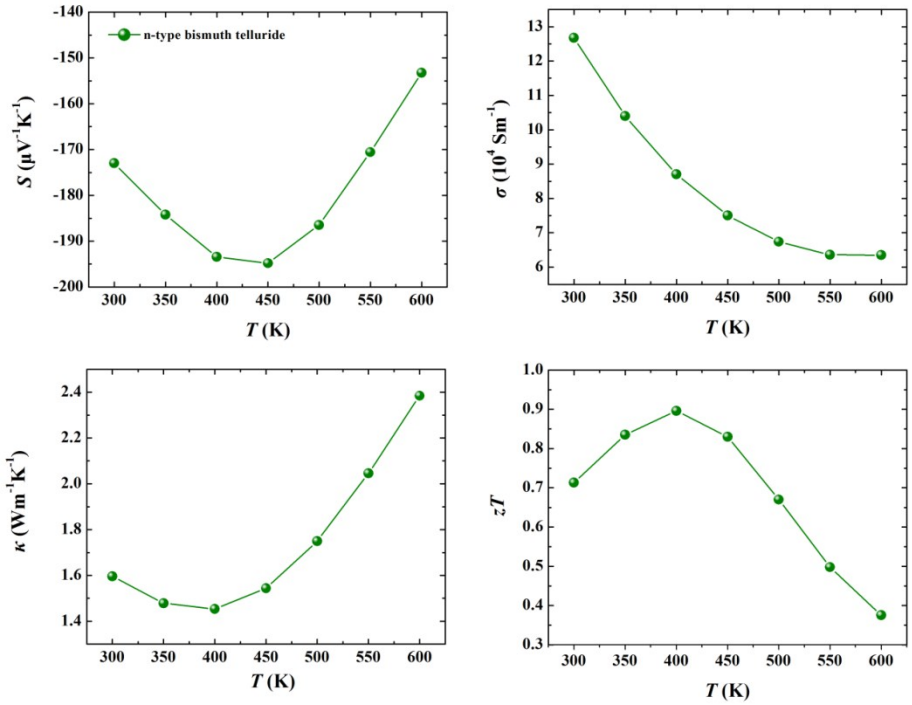

Fig. S1 Temperature dependences of (a) Seebeck coefficient, (b) electrical conductivity, (c) thermal conductivity, and TE figure of merit (zT) for commercial n-type bismuth telluride.

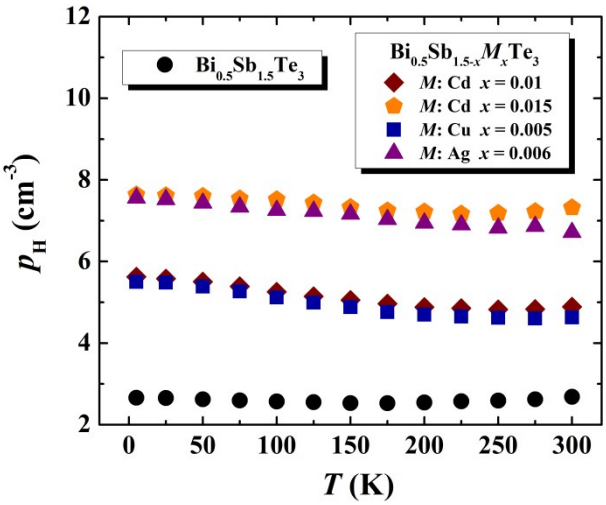

Fig. S2 Temperature dependence of Hall hole concentration (p_H) below 300 K for $Bi_{0.5}Sb_{1.5-x}M_xTe_3$ (M = Cd, Cu, and Ag) samples.

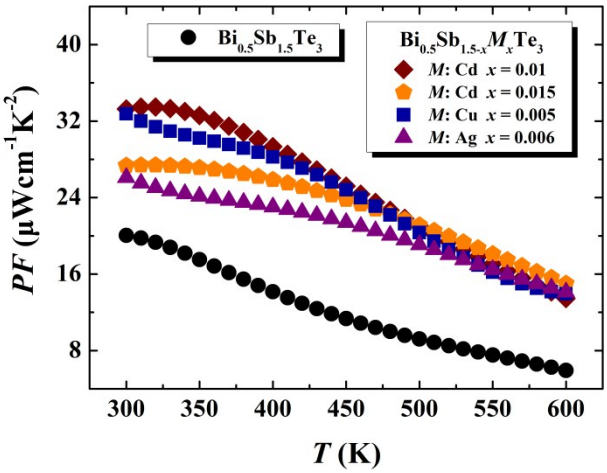

Fig. S3 Temperature dependence of power factor (*PF*) for $Bi_{0.5}Sb_{1.5-x}M_xTe_3$ (*M* = Cd, Cu, and Ag) samples.

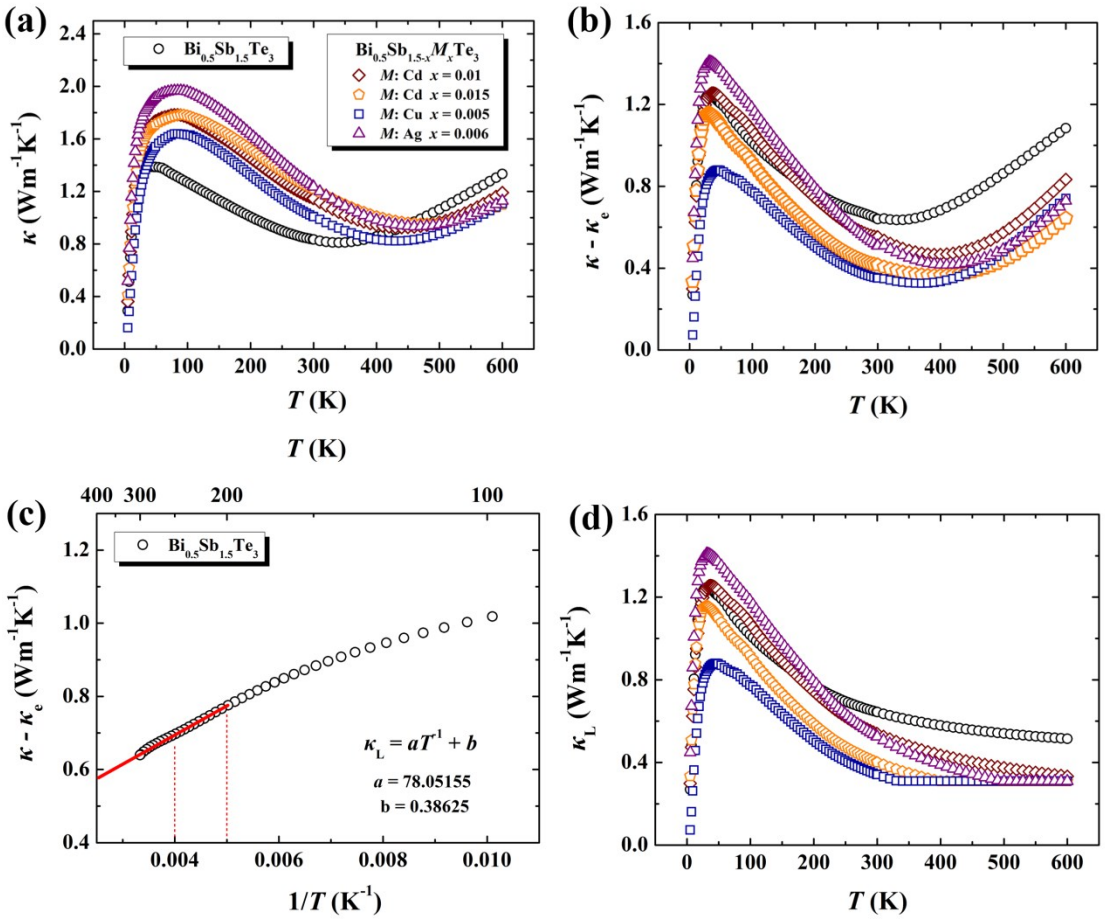

Fig. S4 Temperature dependences of (a) total κ and (b) κ-κ_e for all samples. (c) κ-κ_e as a function of temperature for $Bi_{0.5}Sb_{1.5}Te_3$. The solid line represents the expression of

$\kappa_L = aT^{-1} + b$. (d) Temperature dependence of calculated lattice thermal conductivity (κ_L) for all samples.

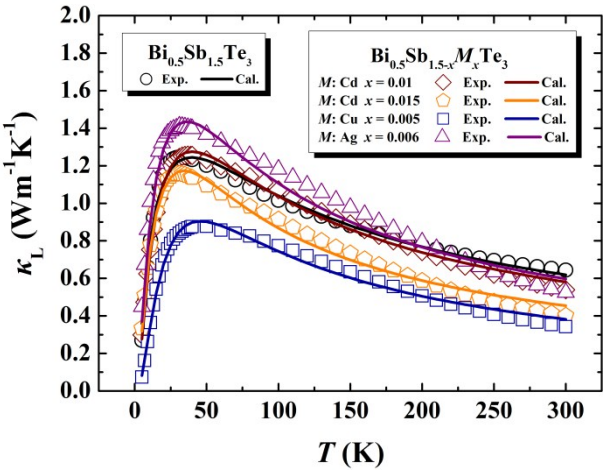

Fig. S5 Temperature dependence of experimental κ_L (symbols) and calculated κ_L (solid lines) by using Debye model for all samples.

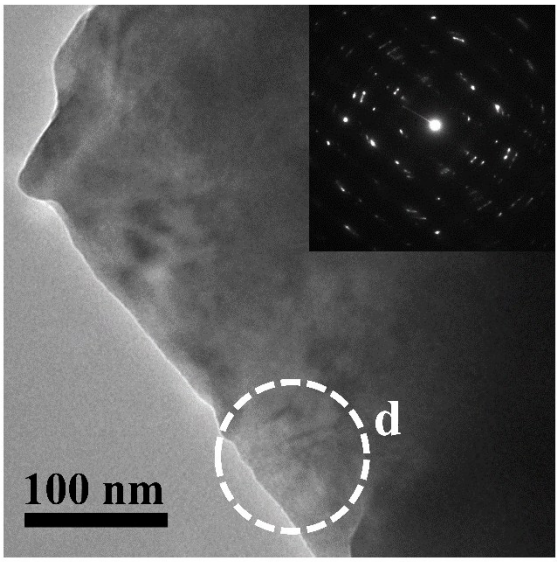

Fig. S6 Low-magnification TEM image for $Bi_{0.5}Sb_{1.49}Cd_{0.01}Te_3$ sample. The insert picture is the electron diffraction pattern of the marked region, in which the nanoscale area in fig. 3d is included.

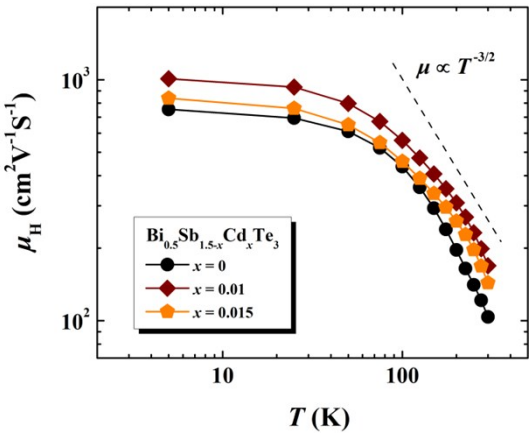

Fig. S7 Temperature dependence of Hall hole mobility (μ_H) below 300 K for Cd-doped $Bi_{0.5}Sb_{1.5}Te_3$ samples.

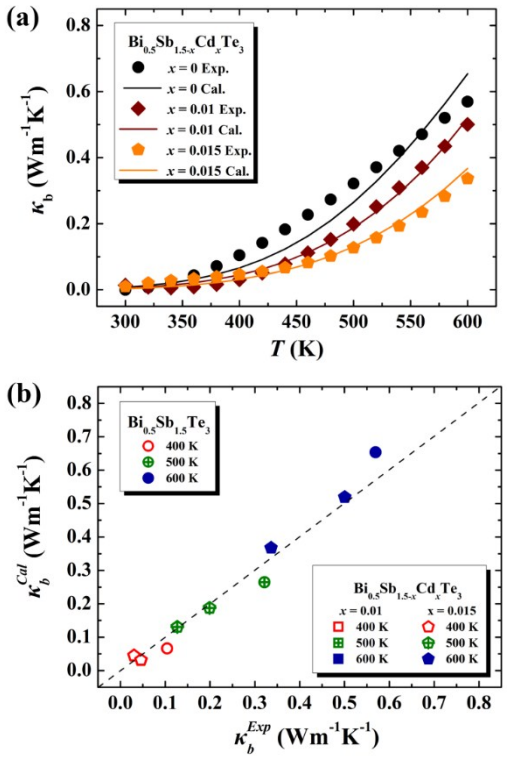

Fig. S8 (a) Temperature dependence of experimental κ_b for $Bi_{0.5}Sb_{1.5-x}M_xTe_3$ (M = Cd, Cu, and Ag) samples. The solid lines represent the numerical fitted κ_b by Equation S1. The fitting parameters B for all samples are shown in Table S3. (b) Experimental

bipolar thermal conductivity (κ_b^{Exp}) and the fitted bipolar thermal conductivity (κ_b^{Cal}). The dash line stands for the relationship of $\kappa_b^{Exp} = \kappa_b^{Cal}$.

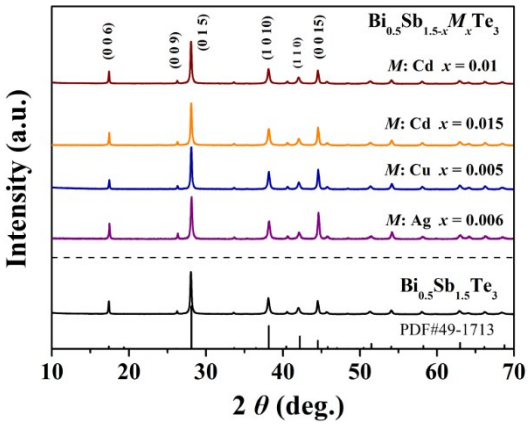

Fig. S9 Powder XRD patterns for $Bi_{0.5}Sb_{1.5-x}M_xTe_3$ (M = Cd, Cu, and Ag) samples.

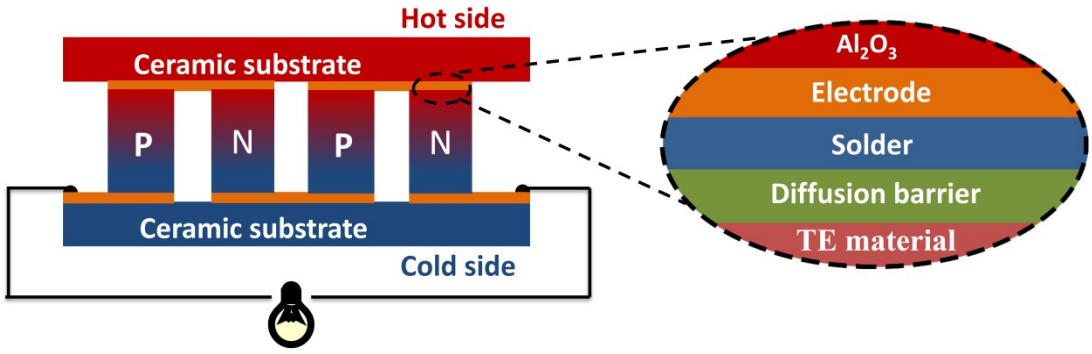

Fig. S10 Schematic graph of our Bi_2Te_3-based modules. Al_2O_3 ceramic is used as the electrically isolated substrate. Cu is used as electrode. SAC305 (96.5% Sn, 3.0% Ag, 0.5% Cu) is the solder. Ni is the diffusion barrier between solder and Bi_2Te_3-based materials.

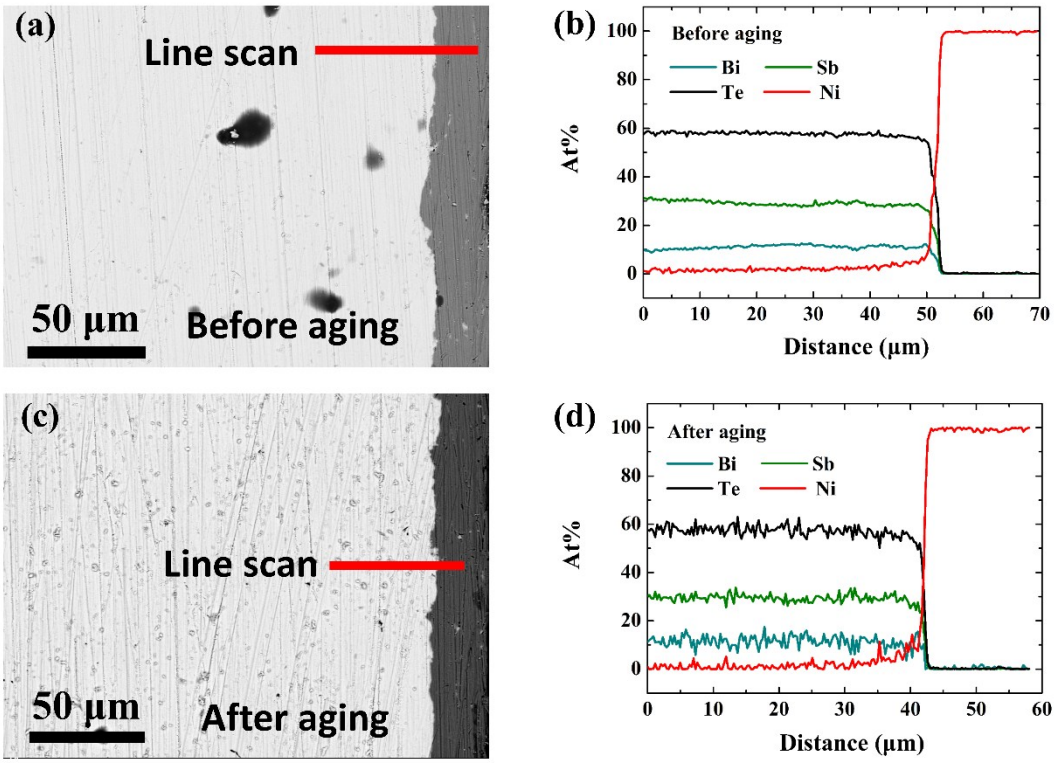

Fig. S11 SEM images of the interfaces between p-type Bi_2Te_3-based material and Ni diffusion barrier (a) before aging and (c) after aging at 250 ˚C for 1 hour, with the respective element line scan shown in (b) and (d) by using EDS. No obvious interdiffusions or chemical reactions are observed after high temperature aging.

Table S1. Calculated Lorenz number L using Equation S2 and fitting parameters for all samples using the expression of $\kappa_L = aT^{-1} + b$ at 200-250 K.

	$Bi_{0.5}Sb_{1.5}Te_3$	$Bi_{0.5}Sb_{1.5-x}M_xTe_3$ (M = Cd, Cu, Ag)			
		Cd: x = 0.01	Cd: x = 0.015	Cu: x = 0.005	Ag: x = 0.006
L	1.6	1.7	1.8	1.7	1.8
a	78.05155	120.38561	105.27573	93.71323	163.32963
b	0.38625	0.1027	-0.05551	-0.01816	-0.01976

Table S2. Fitting parameters for low temperature lattice thermal conductivity by using the Debye model.

	$Bi_{0.5}Sb_{1.5}Te_3$	$Bi_{0.5}Sb_{1.5-x}M_xTe_3$ (M = Cd, Cu, Ag)			
		Cd: x = 0.01	Cd: x = 0.015	Cu: x = 0.005	Ag: x = 0.006

d (μm)	1.755	0.990	1.379	0.179	1.545
P (10^{-41} s^3)	7.409	5.373	6.722	3.754	5.396
U (10^{-18} sK^{-1})	9.903	13.682	18.835	28.775	13.598

Table S3. Calculated parameter A by using Equation 1 and the carrier concentration at 300 K. Parameter B is fitted from the experimental κ_b by using Equation S1 for all $Bi_{0.5}Sb_{1.5-x}M_xTe_3$ (M = Cd, Cu, and Ag) samples.

	$Bi_{0.5}Sb_{1.5}Te_3$	$Bi_{0.5}Sb_{1.5-x}M_xTe_3$ (M = Cd, Cu, Ag)			
		Cd: x = 0.01	Cd: x = 0.015	Cu: x = 0.005	Ag: x = 0.006
A (10^{42} cm^{-6})	3.1	2.5	1.6	1.9	1.7
B (10^3)	1.67	2.6	3.5	2.65	3.7

References

1 C. Chiritescu, C. Mortensen, D. G. Cahill, D. Johnson, P. Zschack, *J. Appl. Phys.*, 2009, **106**, 073503

2 S. Wang, G. Tan, W. Xie, G. Zheng, H. Li, J. Yang, X. Tang, *J. Mater. Chem*., 2012, **22**, 20943.

3 N. Cheng, R. Liu, S. Bai, X. Shi, L. Chen, *J. Appl. Phys.*, 2014, **115**, 163705.